



Impact of Cu doping on ZnO nanoparticles phyto-chemically synthesized for improved antibacterial and photocatalytic activities

IS Okeke · KK Agwu · AA Ubachukwu · M Maaza · FI Ezema 

Received: 1 June 2020 / Accepted: 18 August 2020 / Published online: 4 September 2020
© Springer Nature B.V. 2020

Abstract Green approach was employed to synthesize $Zn_{1-x}Cu_xO$ nanoparticles ($x = 0.0, 0.01, 0.03, \text{ and } 0.05$). The impact of Cu doping on the structure, morphology, and optical properties of ZnO nanoparticles was evaluated using XRD, SEM, and UV-vis spectroscopy, respectively. The XRD analyses confirmed that the samples have hexagonal wurtzite structure. The crystallite size, lattice constants, volume of unit cell,

and bond length of the nanoparticles showed increasing trend as the Cu concentration was increased from 0 to 5% and vice versa for micro-strain and dislocation density. Atomic packing fraction was found to be 74.05% and bond length was between 1.990 and 1.996 Å. SEM image showed spherical, petal, and rod-like shape. Energy band gap (E_g) of samples red shifted from 3.38 to 3.27 eV. The antibacterial results clearly showed that Cu doping in ZnO NPs improved the diameter of inhibition zone across the selected bacteria and exhibited higher degradation efficiency after 100 min of irradiation.

This article is part of the topical collection: Nanotechnology Convergence in Africa

Guest Editors: Mamadou Diallo, Abdessattar Abdelkefi, and Bhekile Mamba

I. Okeke · A. Ubachukwu · F. Ezema
Department of Physics and Astronomy, Faculty of Physical Sciences, University of Nigeria Nsukka, Nsukka, Nigeria

I. Okeke
National Biotechnology Development Agency, FCT, Abuja, Nigeria

K. Agwu
Department of Medical Radiography and Radiological Sciences, Faculty of Health Sciences and Technology, College of Medicine, University of Nigeria Enugu Campus, Enugu, Nigeria

M. Maaza · F. Ezema
Nanosciences African Network (NANOAFNET), iThemba LABS-National Research, 1 Old Faure Road, 7129, P.O. Box 722, Somerset West, Western Cape Province, South Africa

M. Maaza · F. Ezema (✉)
College of Graduate Studies, University of South Africa (UNISA), Muckleneuk ridge, P.O. Box 392, Pretoria, South Africa
e-mail: Fabian.ezema@unn.edu.ng

Keywords *Vernonia amygdalina* · Cu-doped ZnO · Structural study · Optical study · Antibacterial activities · Photocatalytic activities · Nosocomial infection

Introduction

Health care-associated infection (HCAI) also known as nosocomial infection affects significant number of patients without exception and remains one of the leading causes of occupational infection among facility staff. It poses a massive financial responsibility on healthcare services and is linked with elevated patient morbidity and mortality (Donlan 2008). The most frequently reported HCAIs involve 22.8% of ventilator-associated pneumonia and respiratory tract infections, 17.2% of catheter-associated urinary tract infections, and 15.7% of surgical-site infections (Health Protection Agency 2012). Approximately 56% of deaths in neonates are caused by HCAIs, with prevalence rate of 75% in

South-East Asia and Sub-Saharan Africa (World.Health.Organization 2016). In Nigeria, the total HCAI aggregate prevalence in surgical wards is about 45.8% (Kesah et al. 2004). The elevation in prevalence rate of HCAI, drug-resistant bacteria, toxicity, and carcinogenicity of chemical-based disinfectant is a matter of serious concern. Thus, there is a need to develop alternative approaches to formulate a next-generation antibacterial agent from inorganic materials to help mitigate HCAI.

In recent time, the synthesis of metal and metal oxides (like Ag, TiO₂, MgO, CuO, ZnO) has drawn special attention, considering their bacteriocidal and bacteriostatic possible applications in the field of nanomedicine. Among these metal oxides, zinc oxide nanoparticles (ZnO NPs) are quite unique and have been acknowledged as an alternative photocatalyst due to its non-toxicity, high catalytic capability, and economy (Singh et al. 2017). It has also been shown to have high transparency in the visible region of spectrum, electrochemical characteristics, and high thermal stability (Shahid et al. 2018). The photocatalytic activity of ZnO NPs on azo dyes like methyl orange exposed to UV irradiation are very high (Hong et al. 2009). Studies have shown that ZnO NPs with large concentration of surface oxygen vacancies showed improved photocatalytic activities in degradation of Rhodamine B (Wang et al. 2015). Presently, zinc oxide NPs are ZnO NPs considered one of the next-generation materials for biocidal or disinfecting applications and degradation of environmental contaminants because it is associated with higher chemical stability compared to organic disinfectants (Dutta et al. 2012). Prototype ZnO nanoparticles (NPs) have also been used as delivery systems for vaccine and anticancer drugs (Gubin 2009). However, ZnO has a wide direct band gap of 3.37 eV and substantial exciton binding energy of 60 meV (Ahmad et al. 2010). Therefore, ZnO photocatalytic activities are activated upon illumination with UV radiation source. It has been established that ultraviolet and visible light constitute 5–7% and 46% of solar energy, respectively (Bak et al. 2002); thus, it is more economical to develop visible light-activated photocatalyst for bacteria disinfection in surfaces, water, and air.

Often, doping of ZnO with impurity is usually targeted at introducing intra-band gap energy levels that allow ZnO to utilize visible light for photocatalytic application (Samadi et al. 2016). Presently, there is so much attention given to alteration of ZnO NPs by doping it with transition metals like Ag (Wang et al. 2004),

Co (Fabbiyola et al. 2015), Fe (Dao et al. 2016), Ni (Cong et al. 2006), Pd (Zhong et al. 2012), Cr (Li et al. 2009), Ti (Peng et al. 2017), and Mn (Ullah and Dutta 2008) to improve its spectral sensitivity. These studies have demonstrated that transition metals as dopants can affect grain size of ZnO NPs together with its optical properties. Copper is selected as a dopant in this work because it has high electronic conductivity and availability and is relatively cheap (Ca et al. 2011).

Chemical, physical, and biological approaches have been used to synthesize NPs (Kathiresan et al. 2009). However, biological synthesis of NPs has become one of the most preferred methods simply because it is ecofriendly (Anastas and Warner 1998). Bio-synthesized ZnO NPs have been shown to be bio-safe, biocompatible, and desirable for medical applications like drug carriers, cosmetics, and coating of medical materials (Lakshmeesha et al. 2014). Consequently, attention is directed towards plants that have aroma and colors in their leaves for synthesis of NPs because they contain most of the bioactive compounds that can reduce metal salts to metal nanoparticles (Siddiqi and Husen 2017). *Vernonia amygdalina* (VA) well-known as bitter leaf in Nigeria belongs to the *Asteraceae* group. Phytochemical screening result of VA showed high concentration of flavonoids, glycosides, saponins, and alkaloids, (Imaga and Bamigbetan 2013). Flavonoids have been reported to possess antioxidant properties (Edeoga et al. 2005). Lots of work had been carried out on VA towards isolation of secondary metabolites for medicinal purposes; however, there has been no report on synthesis of undoped and Cu-doped ZnO using *V. amygdalina* leaf extracts. Hence, we report an efficient and ecofriendly approach for synthesis of undoped and Cu-doped ZnO NPs, as well as their structural, optical, and morphological properties. Antibacterial activities of the samples were investigated across the selected bacterial: *Staphylococcus aureus*, *Escherichia coli*, and *Pseudomonas aeruginosa* causing nosocomial infections, isolated from wound infections. Moreover, the photocatalytic activities were investigated using methylene blue (MB) as the test contaminant.

Experimental details

Preparation of *Vernonia amygdalina* leaf extract

Fresh leaves of *V. amygdalina* were washed several times with distilled water to get rid of the dust particles,

finely chopped into pieces and then dried in the sun shade at ambient temperature for 14 days to eliminate the residual moisture. The VA extract was prepared using the method of Yedurkar et al. (2016), and 10 g of dried leaves of *V. amygdalina* was added in 250-ml glass beaker along with 150 ml of distilled water. The blend was allowed to boil for 20 min at 60 °C until the color changed from watery to a yellow color. The extract was allowed to cool, then filtered using filter whatman paper, and stored in a refrigerator for subsequent experiments.

Synthesis of undoped and Cu-doped ZnO nanoparticles

All chemicals used for this study were purchased from Sigma-Aldrich and were used without further purification. For synthesis of undoped ZnO and Cu-doped ZnO NPs, the method of Vidya et al. (2013) with some modification was used. Figure 1 is a schematic

representation of processes involved in the syntheses of the nanomaterial using VA extract.

Stoichiometric ratio of zinc nitrate (source of Zn) and copper nitrate (source of Cu) is calculated using $Zn_{1-x}Cu_xO$ (where $x = 0.0, 0.01, 0.03, \text{ and } 0.05$). Each stoichiometric ratio of $Zn_{1-x}Cu_xO$ was added to 50 ml of the extract separately in a 100-ml beaker, at 60–80 °C, and then stirred at 800 rpm for 15 min. Each mixture was allowed to boil at that temperature till it reduces to a yellow paste. The obtained paste was collected in a crucible and placed in an air-heated furnace at 350 °C for 2 h. The obtained powder was grained using pestle and mortar and delicately collected for characterization.

Evaluation of antibacterial activity

The antimicrobial activities of all the samples were tested in vitro across strains of *Staphylococcus aureus*, *Pseudomonas aeruginosa*, and *Escherichia coli* (*E. coli*)

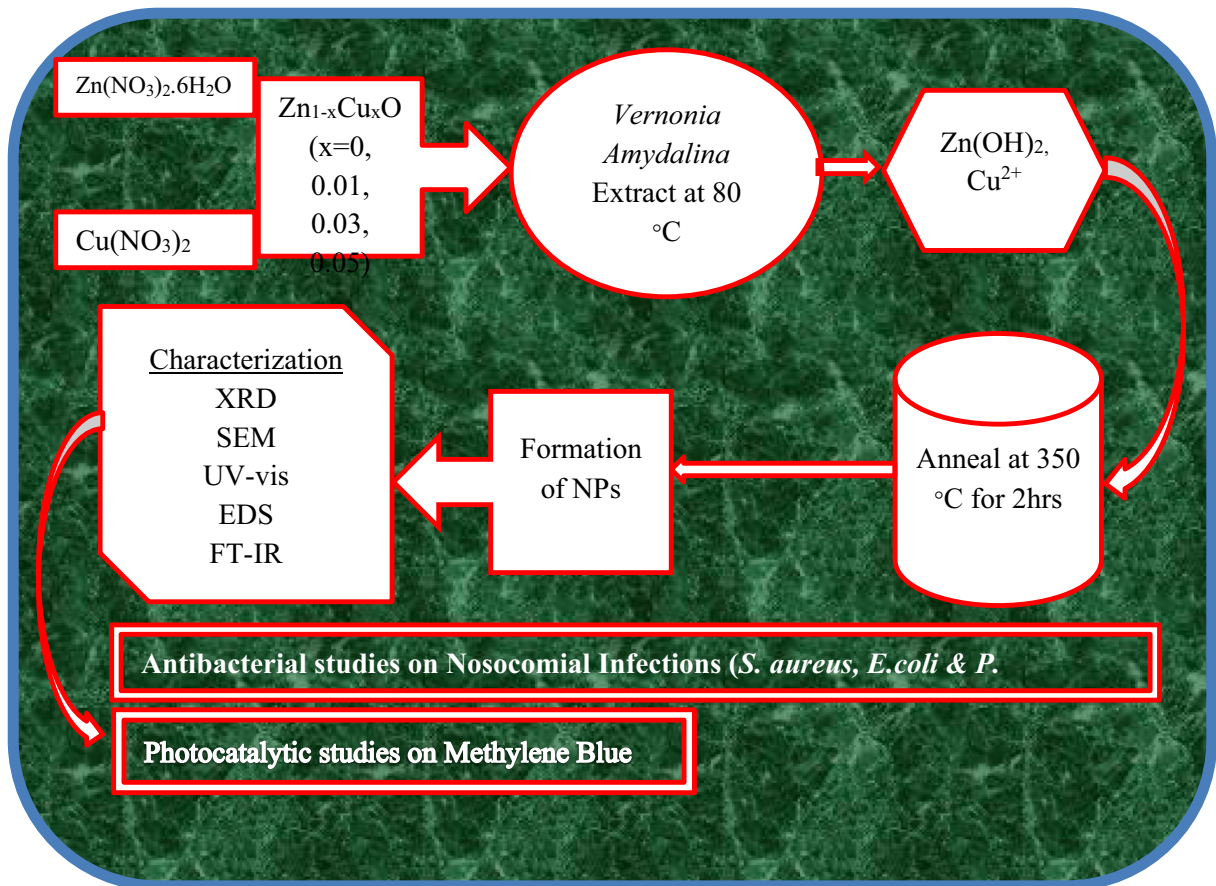


Fig. 1 Schematic diagram for preparation of undoped and Cu-doped ZnO NPs using *Vernonia amygdalina* extract

isolated from wound infection from the National Orthopedic Hospital, Enugu, Nigeria, using agar well diffusion technique (NCCLS 2002). The bacterial dilutions were adjusted to meet the McFarland standard, indicating a bacterial density of 1.5×10^8 CFU/ml. About 25 ml of prepared nutrient agar in a sterile dish was seeded alongside 24 h bacterial cultures by way of dipping a sterile cotton swab into the broth of these microorganisms. For the culture to get absorbed in the medium, the plates were allowed to stand for about 10–15 min. After solidification, 6 mm bores were made in each petri plate using a sterile cork borer and 0.1 ml (100 μ g/ml) of each NPs dissolved in dimethyl sulfoxide (DMSO) was poured into the wells and then incubated for 24 h at 37 °C. DMSO alone without NPs was used as the control (C) test. After incubation, the diameter of inhibition of zones (mm) was measured to assess the antimicrobial activities of samples.

The antimicrobial activities and minimum inhibitory concentration study were approved by the Medical Research Ethics committee, National Orthopedic Hospital Enugu, with IRB/HEC number S.319. Use of the following protective clothing, face masks, hand gloves, laboratory coats, impervious shoe covers and goggles, was strictly complied with all through the experiment.

Determination of the minimum inhibitory concentration

The twofold serial dilutions (SLD) method (Aysaa and Salmanb 2016) was used in determining the minimum inhibitory concentration (MIC) of samples with the highest zone of inhibition for all the isolates. To this, 1 ml of media was appropriated in a test tube, and then 1 ml of test solution was added; consequently, 0.1 ml of the bacterial strains was added to the test tube containing media and test solution. The SLD was performed five times giving concentrations of 20, 10, 5, 2.5, and 1.25 μ g/ml. The control test consists of the inoculated broth supplemented along DMSO alone at the same dilutions. The nutrient broth containing the test samples and control test were incubated for 24 h at 37 °C. The MIC values were considered as the lowest or minimum concentration needed to impede growth of bacteria in the test tube after incubation (showed no turbidity).

Photocatalytic activity test

For the photocatalytic tests, the method of Ganesan et al. (2016) was used. Methylene blue (MB) dye was

prepared by adding 10 mg/l MB in a bottle and stirred for 30 min at room temperature. To the prepared stock, 10 mg of each sample (ZnO, $Zn_{0.99}Cu_{0.01}O$, $Zn_{0.97}Cu_{0.03}O$, and $Zn_{0.95}Cu_{0.05}O$) was added into 50 ml of MB solution separately in a 100-ml beaker. Each mixture was stirred for 50 min in the dark to establish adsorption/desorption equilibrium and then exposed to sunlight. Light intensity and temperature were monitored using Smart Luxmeter (v1.0) and Digital thermometer (MASmed SA, SN: 20033003347), respectively, all through the experimental work. About 2–3 ml of mixture was collected every 20 min, centrifuged at 8000 rpm for 10 min. The collected supernatant was analyzed using UV-visible spectroscopy to measure the degradation of dye. The percentage degradation efficiency (PDE) was estimated using Eq. (1).

$$PDE = \frac{C_0 - C}{C_0} \times 100 \quad (1)$$

where C_0 = concentration at $t = 0$ and C = concentration at different time intervals (0, 20, 40, 60, 80, and 100).

Characterization

The x-ray powder diffraction (XRD) patterns of $Zn_{1-x}Cu_xO$ samples were analyzed using an x-ray diffractometer along Cu ($k\alpha$) radiation ($\lambda = 0.15406$ nm) in a 2θ range of 25–75°. For the surface morphology and particle length investigation, SEM and ImageJ were used. The absorption spectra of the samples were obtained deploying UV-Vis Spectrophotometer at wavelength range of 330–650 nm. The elemental analyzes of the samples were done using energy-dispersive x-ray spectroscopy. The presence and interaction of chemical functional groups in the samples were investigated using FT-IR at the scanning range of 400–4000 cm^{-1} . The antibacterial activities of the samples were done separately in sets of three, and the results are represented as the mean values \pm standard deviation (SD) of each group.

Results and discussions

Structural analysis

Figure 2 is the XRD analyses of all the samples; the results indicated distinctly sharp diffraction peaks

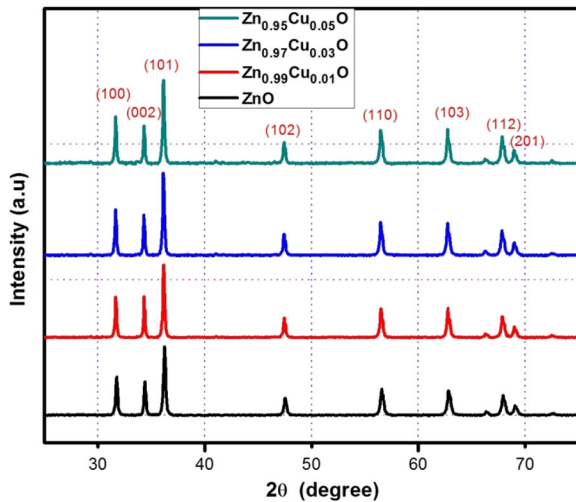


Fig. 2 Comparison of XRD pattern of all the samples ($Zn_{1-x}Cu_xO$, $x = 0.0, 0.01, 0.03, \text{ and } 0.05$)

observed at 2θ angles 31.76, 34.41, 36.25, 47.53, 56.59, 62.85, 67.94, and 69.08 which correspond to the lattice planes (100), (002), (101), (102), (110), (103), (112), and (201). The results confirm that the samples are excellent crystalline in nature along with hexagonal wurtzite structure that is in good agreement with JCPDS card No. 01-079-2205 (Rafaie et al. 2015). The XRD peak positions of all the samples are shown in Table 1.

The impact of Cu doping on the structure of ZnO NPs

The average crystallite size (D) was obtained using the Scherrer equation (Thaweesaenga et al. 2013).

$$D = \frac{k\lambda}{\beta \cos\theta} \tag{2}$$

where $k = 0.9$, $\lambda = 0.154056 \text{ nm}$, β = full width at half maximum (FWHM), θ = Bragg angle. The induced micro-strain (ϵ) was estimated using the equation.

$$\epsilon = \frac{\beta \cos\theta}{4} \tag{3}$$

For geometric structure, lattice parameters (LP) were determined using the following equation.

$$\frac{1}{d^2} = \frac{4}{3} \left[\frac{h^2 + hk + l^2}{a^2} \right] + \frac{l^2}{c^2} \tag{4}$$

where h, k , and l are the miller indices, $a = b$ and c are the lattice constants, and d is the interplanar spacing (Thaweesaenga et al. 2013). Interplanar spacing (d) was estimated using Bragg’s law

$$2d\sin\theta = n\lambda \tag{5}$$

The dislocation density (δ) was calculated applying Eq. 6 (Rouchdi et al. 2017).

$$\delta = \frac{1}{d^2} \tag{6}$$

Once the lattice parameters a and c are determined, other structural parameter like the volume of unit cell (VUC), atomic packing fraction (APF), and bond length (BL) of Zn–O can readily be calculated, respectively, through Eqs. 7, 8, and 9.

$$VUC = 0.866a^2c \tag{7}$$

$$APF = \frac{2\pi a}{3\sqrt{3}c} \tag{8}$$

$$BL = \sqrt{\left(\frac{a^2}{3} + \left(\frac{1}{2}-u\right)^2 2c^2\right)} \tag{9}$$

$u = \frac{a^2}{3c^2} + 0.2$, and it is referred to as a positional parameter (Amrita et al. 2017).

Table 1 XRD peak positions of all the $Zn_{1-x}Cu_xO$ samples compared to standard values

S/n	(hkl) plane (2θ)	(100)	(002)	(101)	(102)	(110)	(103)	(112)	201
1	JCPDS No. 01-079-2205	31.766	34.419	36.251	47.536	56.591	62.852	67.942	69.080
2	ZnO	31.766	34.427	36.254	47.548	56.604	62.886	67.976	69.111
3	$Zn_{0.99}Cu_{0.01}O$	31.689	34.356	36.180	47.480	56.532	62.818	67.906	69.037
4	$Zn_{0.97}Cu_{0.03}O$	31.670	34.338	36.161	47.457	56.110	62.795	67.880	69.015
5	$Zn_{0.95}Cu_{0.05}O$	31.678	34.346	36.163	47.458	56.517	62.801	67.880	69.016

The results for various estimated structural parameters are shown in Table 2. The average crystallite size of ZnO, Zn_{0.99}Cu_{0.01}O, Zn_{0.97}Cu_{0.03}O, and Zn_{0.95}Cu_{0.05}O NPs were found to be 34.40, 39.38, 38.89, and 39.42 nm, respectively. It was noticed that the size of the NPs increases from 34 to 39 nm as Cu content was increased from 0 to 5%. This result is in conformity with the result obtained by the following authors: Chauhana et al. (2010), Chithra and Pushpanathan (2016), and Khan et al. (2017). The addition of Cu does not change the hexagonal wurtzite structure: however, as Cu concentration is increased, the XRD peak position deviates towards a lower 2θ angle which indicates evidence of Cu doping in the ZnO matrix. The deviation in peak positions to the lower 2θ angle may be due to the replacement of Zn²⁺ which has a larger ionic radius (0.74 Å) by Cu²⁺ with a smaller ionic radius (0.73 Å) (Vegard 1921). The intensity of the diffraction increases with increment in Cu concentration, which also confirms the presence of Cu in the ZnO structure. In addition, no Cu peak was noticed in the XRD patterns of the doped samples, thereby, suggesting incorporation of Cu ion into the Zn lattice site rather than the interstitial site. This could be linked to the negligible difference in ionic radii Zn²⁺ and Cu²⁺.

The calculated crystal defect parameters like the induced micro-strain and dislocation density decreased with rise in Cu concentration. This finding implies that the higher the Cu content (up to 5%) in ZnO nanostructure, the smaller the internal stress, and it is consistent with theoretical (using first principle calculations) results obtained by Ma et al. (2019).

The ZnO nanostructure possesses lattice constants $a = 3.250$ and $c = 5.210$ Å (George et al. 2009). In this study, for undoped ZnO, the calculated lattice constant were $a = 3.250$ Å and 5.307 Å. However, it was observed that the lattice parameter “a” swiftly increased to

0.22%, 0.30%, and 0.25% at 1, 3, and 5% Cu doping, respectively. In the same way, “c” also instantly increased to 0.22%, 0.30%, and 0.26% at 1, 3, and 5%, respectively, as shown in Fig. 3. The observed increment in lattice constants confirms that Cu ion was successfully doped in the ZnO matrix and could be linked to the replacement of Zn²⁺ by Cu⁺ and Cu²⁺ ions (Labhane et al. 2015). The VUC increased to about 0.8% as the Cu concentration was increased from 0 to 5%, and the result suggests that ionic radii of Cu ions expanded the unit cell of the ZnO NPs by 0.8%. The calculated atomic packing fraction (APF) of each samples was found to be 74.05%, and this result is in accord with the 74% obtained by Amrita et al. (2017), thereby, confirming that all the samples have a hexagonal closed pack structure. The calculated BL is between 1.990 and 1.996 Å which is in agreement with the reported Zn–O BL 1.9767 Å (Ju-nam and Lead 2008).

Morphological analysis

SEM was employed to analyze the impact of different concentrations of Cu on the particle length and surface morphology of ZnO. The micrograph of all the samples is displayed in Fig. 4(a, b, c, and d). The results reveal that the surface morphology of ZnO NPs altered with increase in Cu concentration. This result is consistent with the result obtained by Labhane et al. (2015), for 1, 2, and 3% Cu-doped ZnO using co-precipitation technique. For ZnO and Zn_{0.99}Cu_{0.01}O, the micrograph displayed spherical and petal-like-shaped NPs while Zn_{0.97}Cu_{0.03}O and Zn_{0.95}Cu_{0.05}O showed rod-like-shaped NPs. It was observed that the grain size increases with increment in Cu concentration as shown in grain size distribution (PLD) in Fig. 5(a, b, c, and d). The PLD of all the samples, ZnO, Zn_{0.99}Cu_{0.01}O, Zn_{0.97}Cu_{0.03}O, and Zn_{0.95}Cu_{0.05}O, had mean grain size of 427, 441,

Table 2 Structural data of Zn_{1-x}Cu_xO samples

S/n	Sample code	NPs size (nm)	Induced strain (%)	Lattice constant (Å)		Dislocation density	Volume of unit cell (Å) ³	Atomic packing factor (%)	Bond length (Å)
				a = b	c				
1	ZnO	34.31	0.3837	3.250	5.307	8.49×10^{-4}	48.55	74.05	1.990
2	Zn _{0.99} Cu _{0.01} O	39.38	0.3208	3.257	5.319	6.45×10^{-4}	48.89	74.05	1.994
3	Zn _{0.97} Cu _{0.03} O	38.89	0.3268	3.260	5.323	6.61×10^{-4}	48.98	74.05	1.996
4	Zn _{0.95} Cu _{0.05} O	39.42	0.3218	3.258	5.321	6.44×10^{-4}	48.94	74.05	1.995

Fig. 3 Lattice parameters “a” and “c” of all the samples

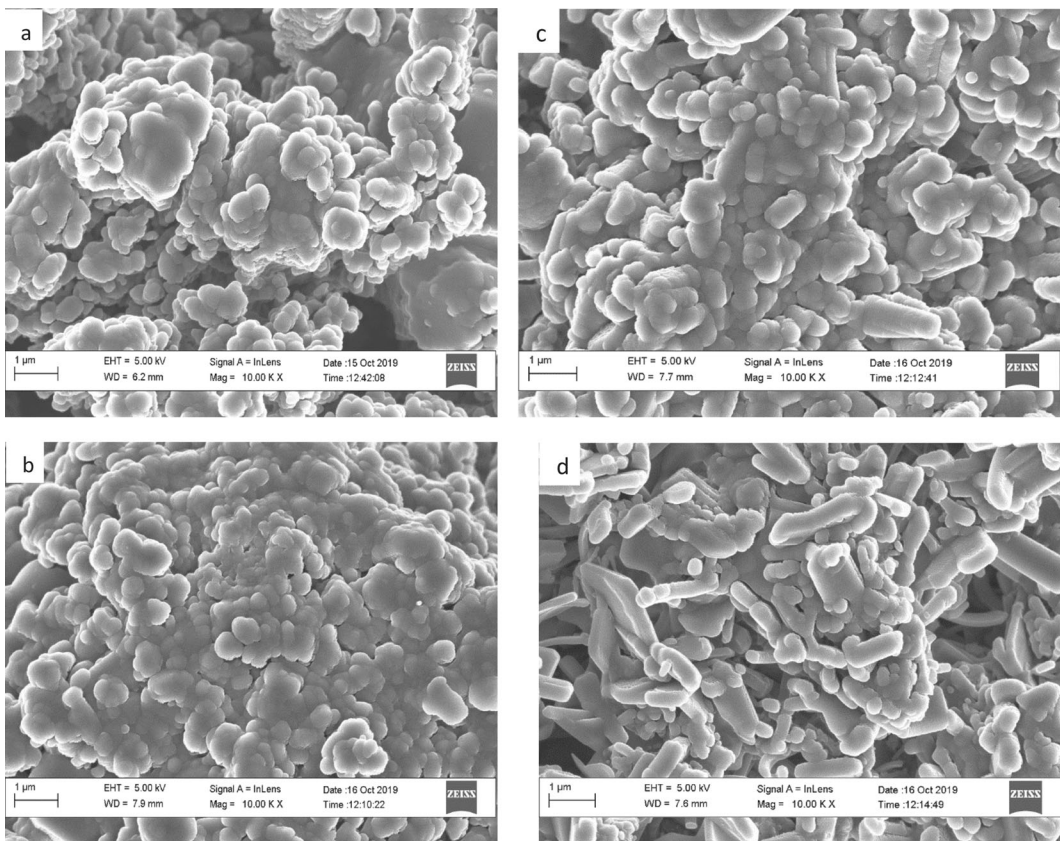
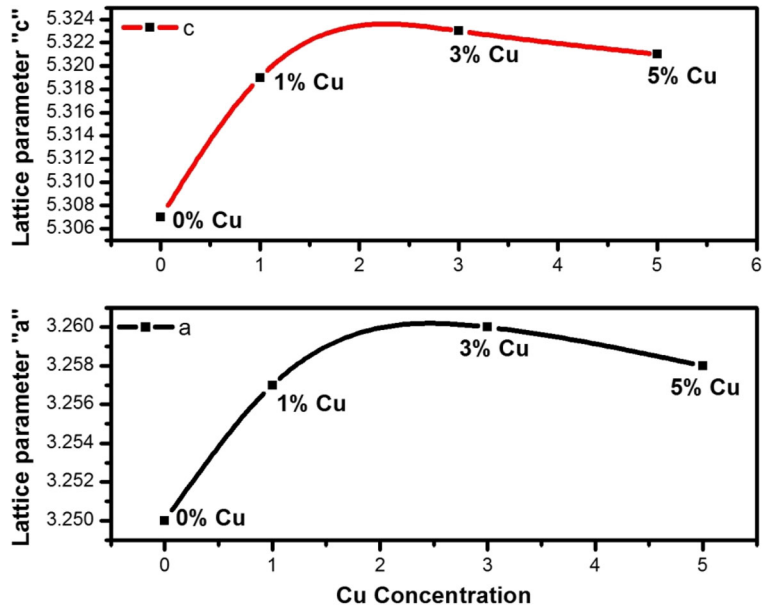


Fig. 4 **a** The SEM micrograph of ZnO sample. **b** The SEM micrograph of Zn_{0.99}Cu_{0.01}O sample. **c** The SEM micrograph of Zn_{0.97}Cu_{0.03}O sample. **d** The SEM micrograph of Zn_{0.95}Cu_{0.05}O sample

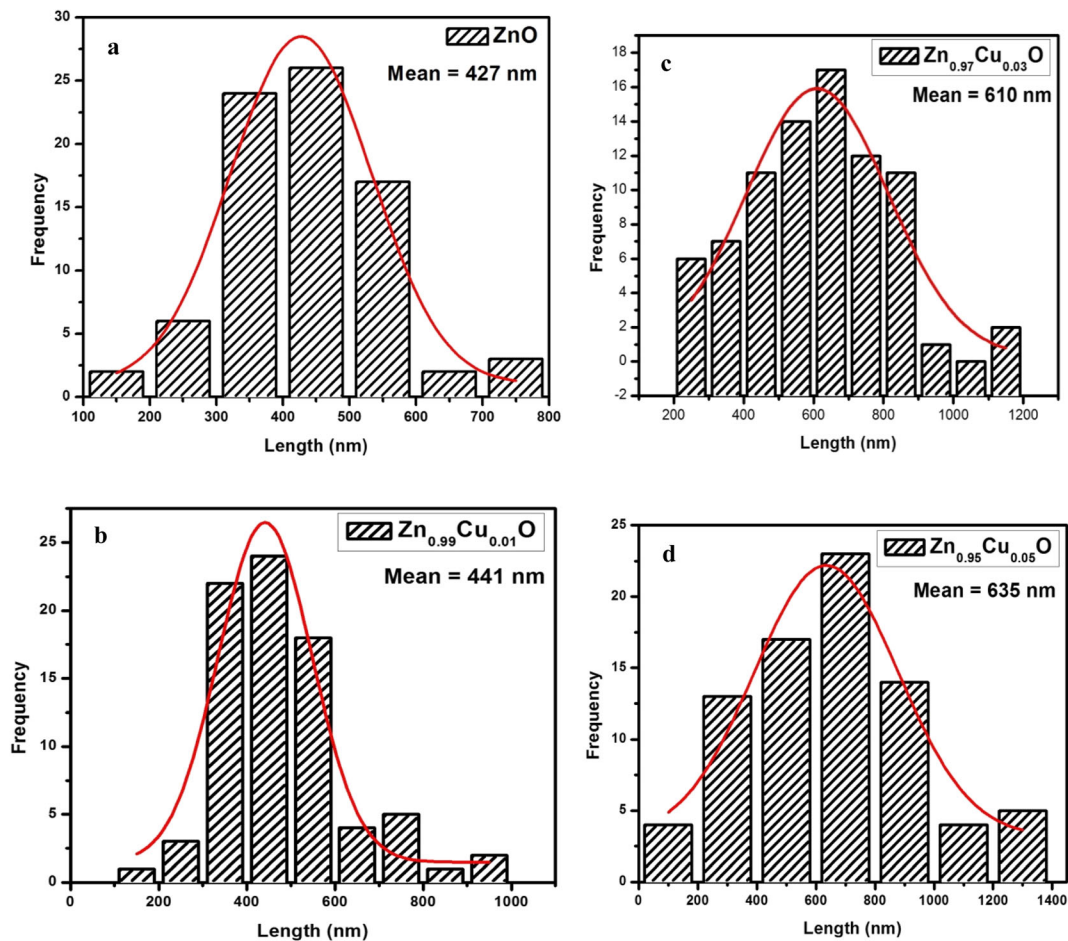


Fig. 5 a Grain size distribution of ZnO sample. b Grain size distribution of $Zn_{0.99}Cu_{0.01}O$ sample. c Grain size distribution of $Zn_{0.97}Cu_{0.03}O$ sample. d Grain size distribution of $Zn_{0.95}Cu_{0.05}O$ sample

610, and 635 nm, respectively. Furthermore, the ZnO showed lower agglomeration and smaller grain size compared to $Zn_{0.99}Cu_{0.01}O$, $Zn_{0.97}Cu_{0.03}O$, and $Zn_{0.95}Cu_{0.05}O$. This suggests that Cu aided the development of secondary particles through agglomeration of elementary particles.

Energy-dispersive analysis

The elemental composition analysis of the samples was done using EDX. Figure 6 showed sharp signals of zinc (Zn) and oxygen (O) for undoped ZnO which affirms the formation of ZnO NPs. The following elements, Zn, O, and Cu signals, were observed in $Zn_{0.99}Cu_{0.01}O$, $Zn_{0.97}Cu_{0.03}O$, and $Zn_{0.95}Cu_{0.05}O$ NPs which corroborate that Cu was successfully doped in ZnO NPs. However, carbon (C) and traces of elements like silicon (Si),

chlorine (Cl), and potassium (K) were also observed in the EDS of the samples. The presence of these elements confirms the involvement of *V. amygdalina* phytochemicals in reducing and capping of the synthesized samples. The elemental analysis of *V. amygdalina* extract was investigated by Alara et al. (2019) using EDS. The results confirmed presence of C and O in high quantity while elements like Cl, K, O, and Si are in moderate quantity. The presence of C and other elements in the EDX spectral of the samples indicates the presence of stabilizing agents (Bala et al. 2014). These elements originated from plant biomass.

UV-visible spectroscopy

For the energy band gap (E_g) studies, UV-visible spectroscopy technique was used. The spectra of the samples

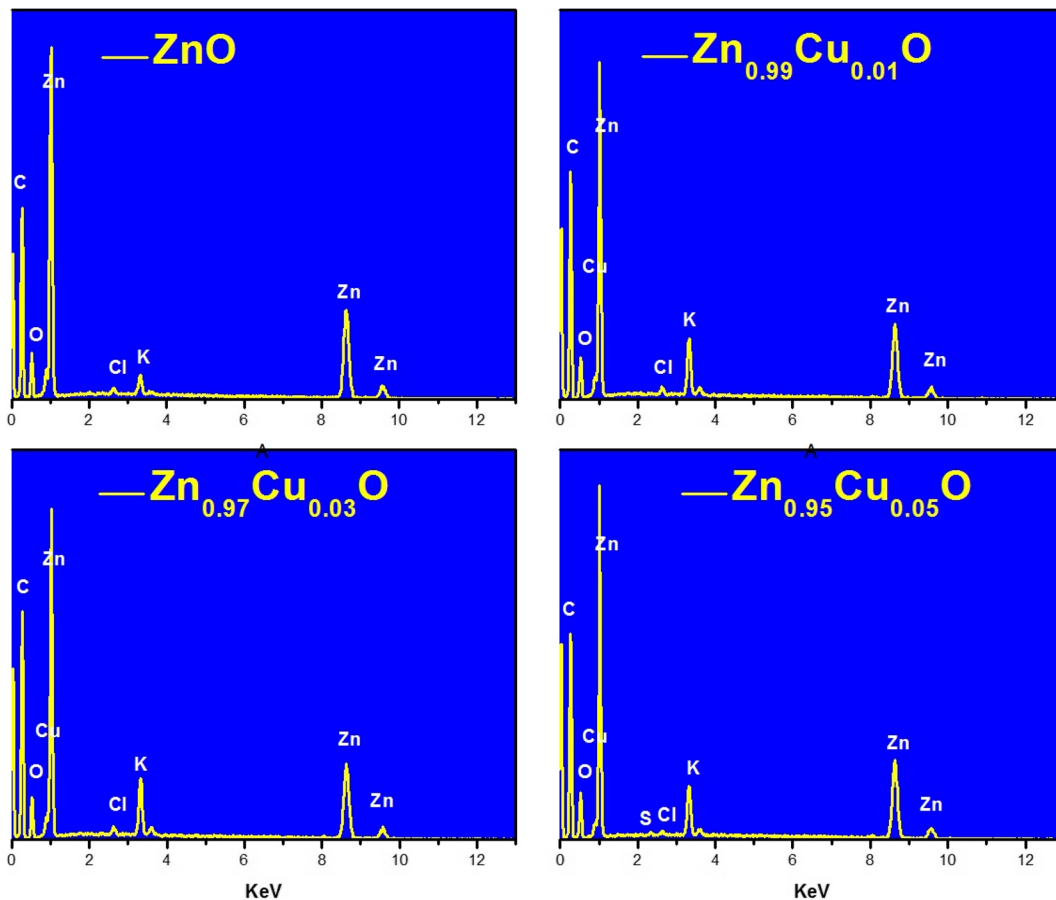


Fig. 6 The EDX spectra of all the samples

were taken in the range of 330 to 620 nm at ambient temperature, and their E_g was determined using Tauc-plot relation (10),

$$(\alpha h\nu)^{1/2} = A(h\nu - E_g) \tag{10}$$

where α , E_g , $1/2$, and A are the absorption coefficient, energy band gap, transition type (direct band gap), and proportionality constant, respectively (Kaur et al. 2015). The E_g of the NPs was calculated by plotting $(\alpha h\nu)^{1/2}$ versus $(h\nu)$ and taking the intercept of the extrapolation to the photon energy axis. Figures 7 and 8 show absorbance spectra and E_g of the samples. The absorption edge of ZnO, $Zn_{0.99}Cu_{0.01}O$, $Zn_{0.97}Cu_{0.03}O$, and $Zn_{0.95}Cu_{0.05}O$ NPs was found to be 371, 375, 377, and 380 nm, respectively. This suggests that the higher the Cu concentration in ZnO (up to 5%), the higher the absorption edge in the UV-visible region. Additionally, the E_g of the samples decreased with the increase in concentration of Cu as shown in Figure 8. These

findings suggest that Cu induced a redshift in the E_g of ZnO NPs. The induced redshift ($\Delta E_g = 0.11$ eV) also confirms the substitution of Cu ion in the ZnO lattice structure and could be attributed to the formation of intraband energy level in the E_g of ZnO. The reduction in the E_g was due to many body effects on the conduction band and valence band (Hamberg and Granqvist 1986). The observed decrease in E_g of doped samples conforms to the findings reported in Sajjad et al. (2018).

Fourier transform infrared (FT-IR) spectroscopy

FT-IR spectroscopy analyzer was used in identifying different functional groups in the samples and was analyzed at spectrum range of 4000–500 cm^{-1} wave number in percent transmittance mode, as shown in Figure 9. Distinct peaks were noticed at peculiar wave number and maintained the same trend in all the samples. A strong and intense absorption band centered between 3525 and 3481 cm^{-1} is accredited to the hydroxyl group

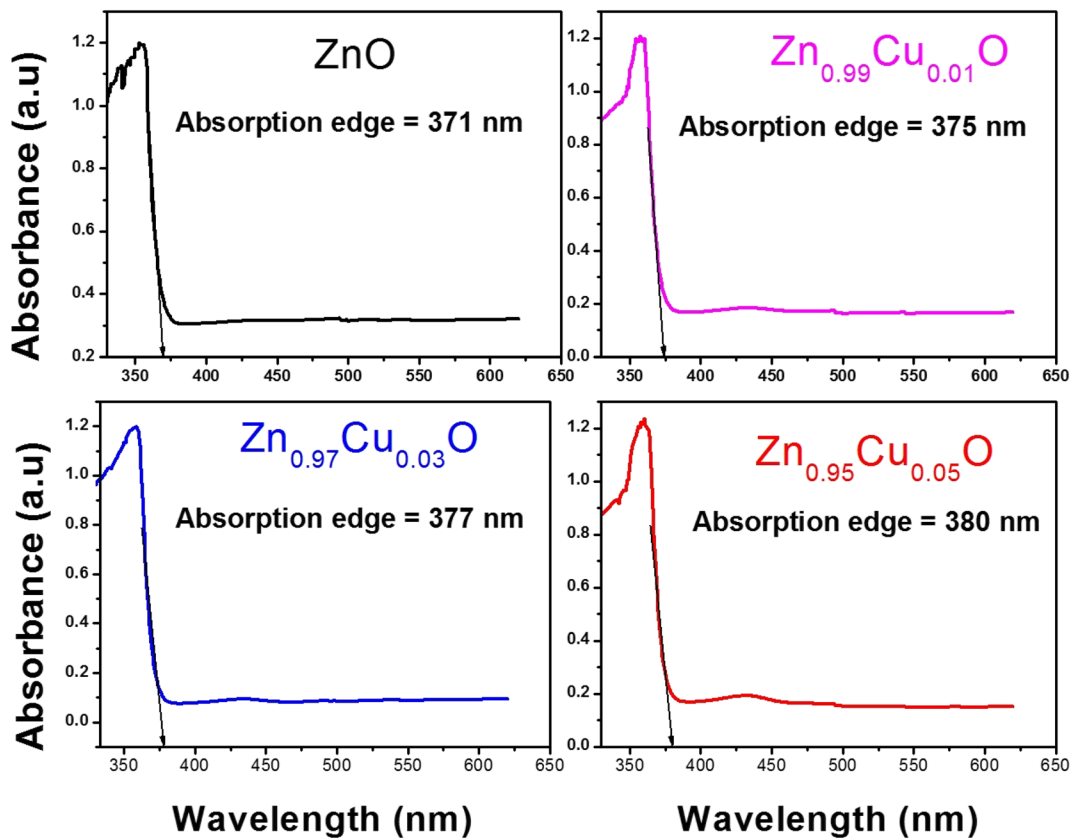


Fig. 7 Absorbance spectra of $Zn_{1-x}Cu_xO$ samples

(OH) stretching vibrations due to water and phenols (Parthiban and Sundaramurthy 2015). The observed medium absorption bands in the region between 1641 and 1542 cm^{-1} was as result as of aromatic C=C ring and C=O stretch in polyphenols while the strong peak band between 1376 and 1371 cm^{-1} is traced to CH–H bending of methyl which can be associated with the presence of proteins (Senthilkumar and Sivakumar 2014; Handago et al. 2019). The peak between 825 and 824 cm^{-1} is linked to C–H. Finally, Peaks between 639 and 505 cm^{-1} is the characteristic absorption of Zn–O bond (Bhuyan et al. 2005). FT-IR spectra analyses demonstrated that the presence of significant phenolic group of molecules in *V. amygdalina* extract are responsible for the reduction process while the amino acids and amide linkages are associated with capping and stabilization of the samples.

Antimicrobial activities of the samples

Table 3 indicates the diameter of inhibition zones (DOIZs) of all the samples across selected gram-

positive and gram-negative bacteria causing nosocomial infections. The investigation was done using Agar well diffusion method. It is fascinating to note that the bacterial pathogens were all sensitive to the samples. However, gram-negative bacteria were more sensitive to the samples; this may be due to the electrostatic attractive interaction between positively charged Zn^{2+} and negatively charged cell wall line of a gram-negative bacteria. Moreover, the cell wall of gram-positive bacteria has a thick layer of peptidoglycan 20–80 nm while that of gram-negative bacteria has a thin peptidoglycan 2–3 nm (Hajipour et al. 2012). Thus, it was easier for the synthesized NPs to interact more with gram-negative bacteria. Figure 10 shows the image of DOIZs for all the samples against selected bacteria causing nosocomial infections. It is evident that Cu doping in ZnO NPs gave higher DOIZs across the selected pathogens: *Staphylococcus aureus* (21 mm), *E. coli* (24 mm), and *Pseudomonas aeruginosa* (25 mm). The improvement in DOIZs observed in 3 and 5% Cu doping could be closely associated to the induced redshift by Cu ion in the energy band gap of ZnO NPs and the observed

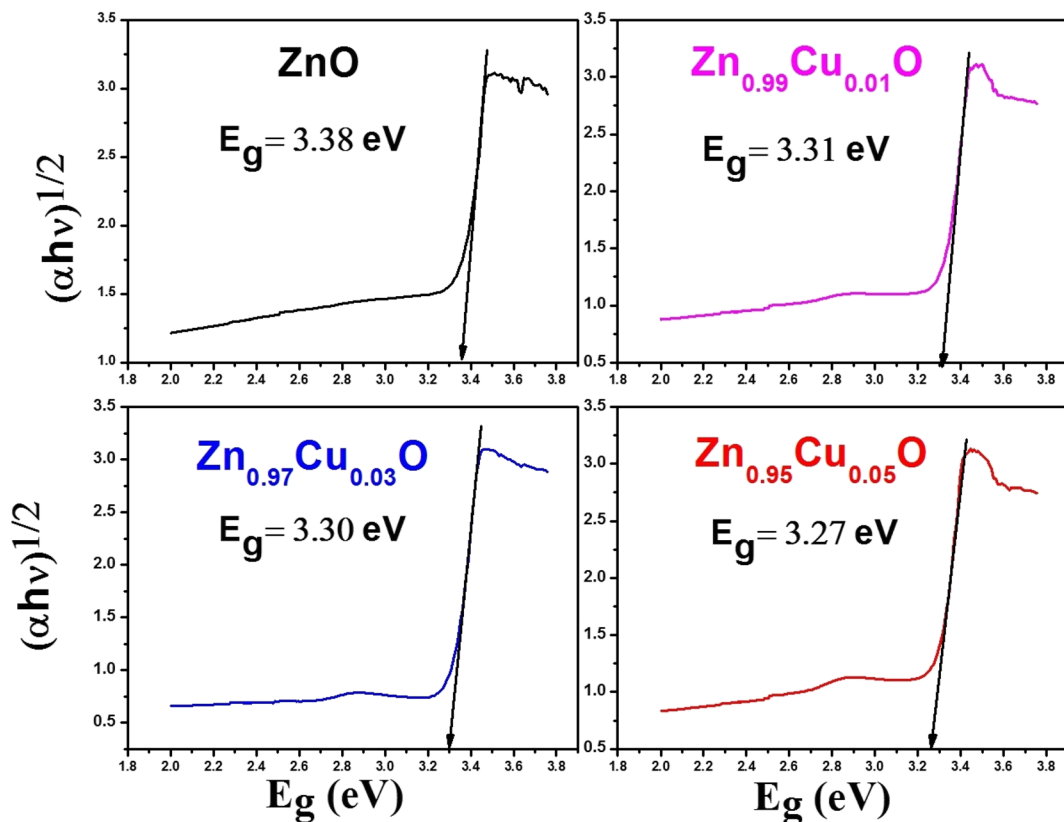


Fig. 8 Energy band gap (E_g) of Zn_{1-x}Cu_xO samples

particle agglomeration. The MIC for Zn_{0.95}Cu_{0.05}O against *S. aureus* and *E. coli* was found to be 10 and 2.5 $\mu\text{g/ml}$ respectively, while Zn_{0.97}Cu_{0.03}O against *P. aeruginosa* was found to be 5 $\mu\text{g/ml}$.

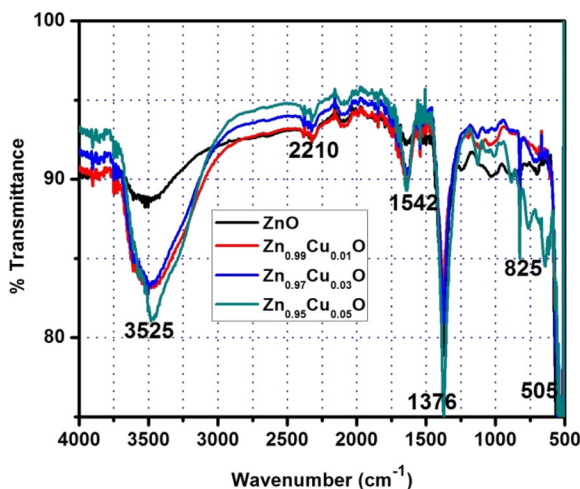


Fig. 9 FT-IR spectra of Zn_{1-x}Cu_xO samples synthesized using *Vernonia amygdalina*

The mechanisms of antibacterial activities of ZnO could be related to size of the NPs, surface defects, zinc ion (Zn^{2+}) release, and oxidative stress. The average cell wall diameter of a bacterium is about 1 μm (Bacterial cell structure n.d.) and about 250 times bigger than a ZnO NPs (Yousef and Danial 2012). This makes it easy for these NPs to adhere and penetrate cell walls of the bacteria, leading to destruction and death of the microorganism. Surface defects in ZnO NPs creates space for ZnO NPs to interact with microorganism (Nirmala and Pandian 2007), due to potential reactive sites. This interaction could occur alongside the basic elements in the outer cell membrane and can possibly degrade or induce structural change that could lead to cell death. The release of Zn^{2+} in medium plays a vital part in the toxic effects of ZnO NPs (Song et al. 2010). The released Zn^{2+} causes destruction to bacteria by disrupting amino acid metabolism and enzymatic system of the microorganism (Sirelkhatim et al. 2015). Zinc and copper ions crosslink with nucleic acid strands by interacting with the deoxyribonucleic acid (DNA) of the microorganism. This results in denaturation of

Table 3 Antibacterial activities of the samples against bacteria causing nosocomial infections

S/n	Sample code	Diameter of inhibition zones (mm) ± standard deviation			
		Gram-positive bacterium <i>Staphylococcus aureus</i>	Gram-negative bacteria <i>E. coli</i> <i>Pseudomonas aeruginosa</i>		Control (DMSO)
1	ZnO	18 ± 0.6	20 ± 0.3	23 ± 0.6	–
2	Zn _{0.99} Cu _{0.01} O	20 ± 0.9	23 ± 0.3	24 ± 0.5	–
3	Zn _{0.97} Cu _{0.03} O	21 ± 0.3	21 ± 0.6	25 ± 0.3	–
4	Zn _{0.95} Cu _{0.05} O	21 ± 0.8	24 ± 0.5	24 ± 0.3	–

protein and outright demolition to the bacterial cell (Ijaz et al. 2017). The oxidative stress approach could be due to the potentiality of ZnO NPs to induce reactive oxygen species (ROS) like superoxide (O_2^-), and hydroxyl

(OH⁻) and hydrogen peroxide (H₂O₂) radicals on its surfaces via photocatalytic process. Hydrogen peroxide radicals can enter cell wall membrane of the bacteria and cause damage or cell death (Sirelkhatim et al. 2015).

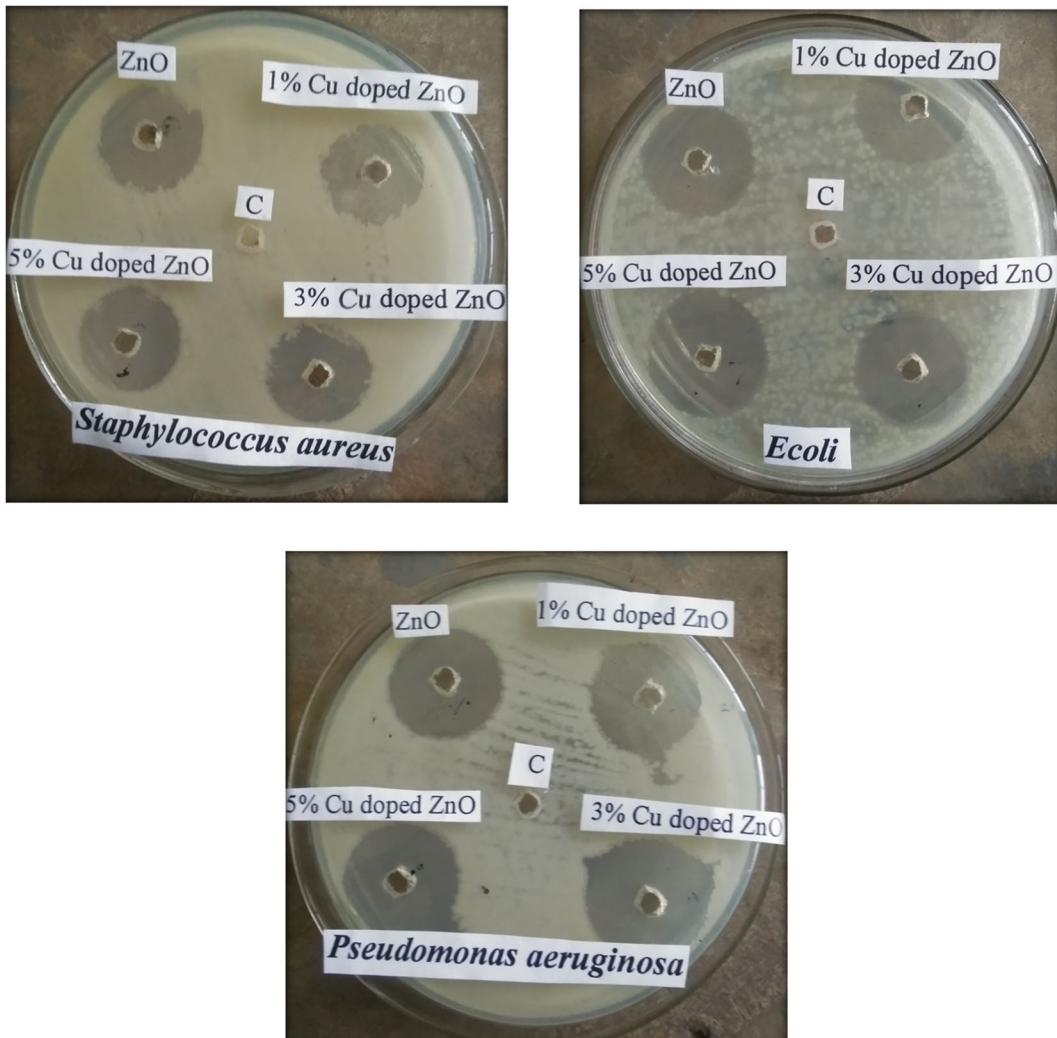
**Fig. 10** Diameter of inhibition zones of all the samples against selected bacteria causing nosocomial infection

Table 4 MIC results of the Samples with highest diameter of inhibition zones

S/n	Bacteria strain	MIC of the samples (µg/ml) against bacteria			
		ZnO	Zn _{0.99} Cu _{0.01} O	Zn _{0.97} Cu _{0.03} O	Zn _{0.95} Cu _{0.05} O
	<i>Staphylococcus aureus</i>	–	–	–	≥ 10
	<i>E. coli</i>	–	–	–	≥ 2.5
	<i>Pseudomonas aeruginosa</i>	–	–	≥ 5	–

Table 4 is the MIC result for samples with highest DOIzs across gram-negative and gram-positive bacteria. Their MIC was investigated using twofold serial dilutions method.

Photocatalytic activities

The photocatalytic percentage degradation efficiency (PDE) of the samples on MB dye solution was investigated under distinct intervals of time (0, 20, 40, 60, 80,

and 100 min) using sunlight as a source of irradiation. Methylene was utilized as test contaminant because the International Standard Organization (International Standard Organization 2010) recognized it as standard for measuring self-cleaning activity of photocatalytic semiconductor. The absorption spectrum of each sample was recorded every 20 min. All the samples showed degradation of MB solution as time increases from 0 to 100 min. The degradation was also observed in the color changes; as the irradiation time increases, the

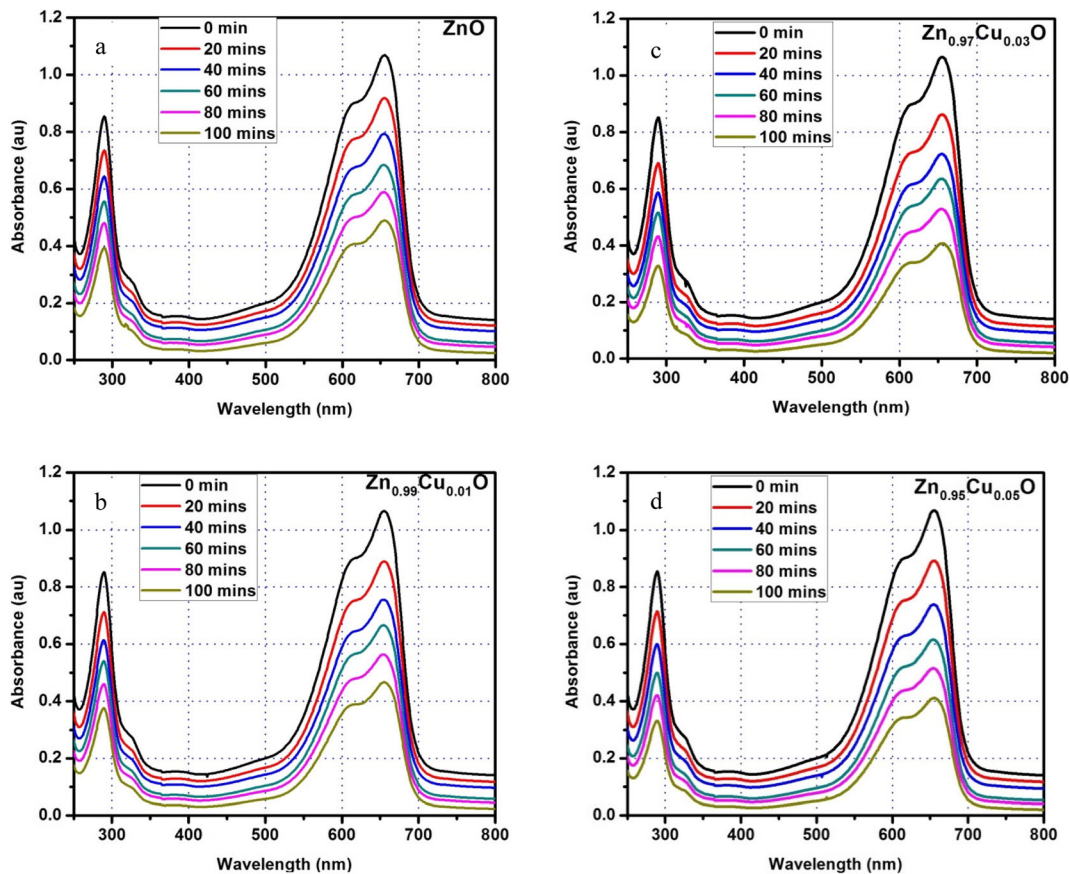


Fig. 11 a The absorption spectra of ZnO sample on MB solution. b The absorption spectra of Zn_{0.99}Cu_{0.01}O sample on MB solution. c The absorption spectra of Zn_{0.97}Cu_{0.03}O sample on MB solution. d The absorption spectra of Zn_{0.95}Cu_{0.05}O sample on MB solution

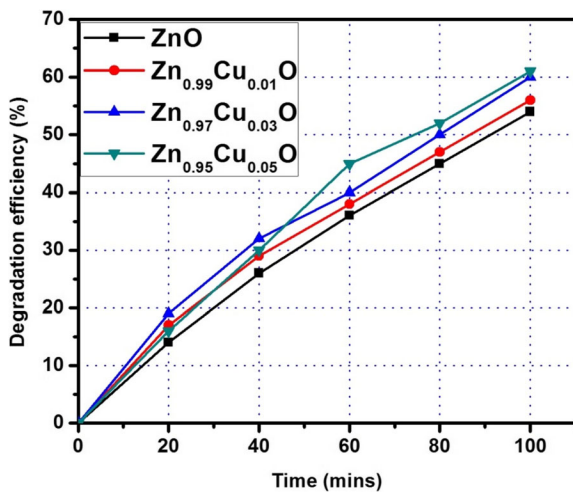


Fig. 12 PDE of all the samples after 100 min

decolorization also increases. Figure 11(a, b, c, and d) also demonstrated that the absorption peaks decreases with the lapse of time, indicating photocatalytic activities of the samples.

Figure 12 indicated that the PDE of the samples increases with increment in dopant concentration, and this finding is in agreement with results obtained by Mohan et al. (2012). After 100 min of exposure, ZnO, Zn_{0.99}Cu_{0.01}, Zn_{0.97}Cu_{0.03}O, and Zn_{0.95}Cu_{0.05}O NPs had 54%, 56%, 60%, and 61% PDE, respectively.

The photocatalytic rate of organic compound and photocatalyst was estimated using pseudo first-order kinetics (Yadav et al. 2007) as shown in Eq. 11.

$$\ln C = -kt + \ln C_0 \quad (11)$$

Rearranging Eq. 11 gives

$$\ln \frac{C_0}{C} = kt \quad (12)$$

where k = kinetic rate constant and can be estimated precisely from the linear fit from plot of $\ln \frac{C_0}{C}$ vs exposure time. From Fig. 13a, it is noticeable that an increase in Cu concentration (up to 5%) in ZnO structure improved the photocatalytic rate. Figure 13b shows reaction kinetics of MB in the presence of the samples (a plot of $\ln \frac{C_0}{C}$ vs exposure time). The kinetic rate constant (k) and their correlation coefficients (R^2), PDE, and energy band gap are shown in Table 5. It is quite obvious that Zn_{0.97}Cu_{0.03}O and Zn_{0.95}Cu_{0.05}O showed better kinetic rate constants compared to ZnO NPs, and this observation suggests that doping up to 5% of Cu in ZnO NPs

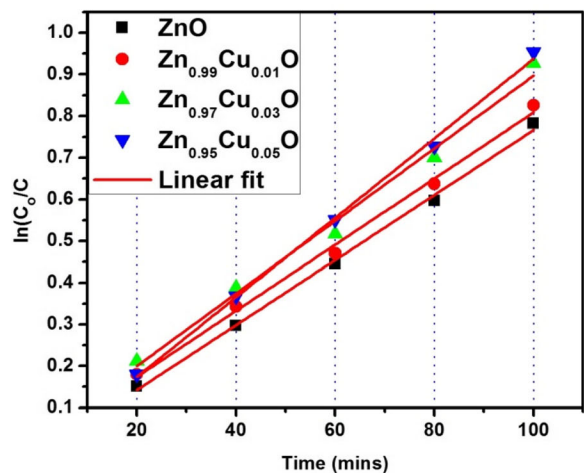
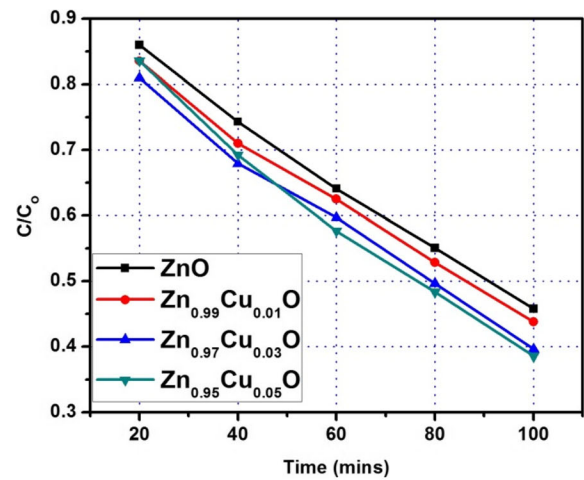


Fig. 13 a Photodegradation rate of MB in the presence of the of the samples. b Reaction kinetics (plot of $\ln(C_0/C)$ against exposure time) of MB in the presence of the of the samples

can improves its photocatalytic activities. The improved PDE and k observed in Zn_{0.97}Cu_{0.03}O and Zn_{0.95}Cu_{0.05}O can be linked to the observed shrinkage in their energy band gap. Furthermore, it can also be linked to the large number of defects like zinc interstitial (Zi_i) and oxygen vacancies (V_o) generated by the Cu ions in ZnO matrix.

The photocatalytic mechanism is initiated when ZnO absorbed a photon ($h\nu$) that equals or is greater than its energy band gap, and electron moves from the valence band (VB) to the conduction band (CB), thus creating electrons (e^-) and a positive hole (h^+).



The electrons and holes have strong oxidizing and reducing power and when they reach the surface or

Table 5 The energy band gap, percentage degradation efficiency, kinetic rate constant, and correlation coefficients of the samples

S/n	Sample	Energy band gap (eV)	PDE (%) after 100 min	Kinetic rate constant k (min ⁻¹)	Correlation coefficients R^2
1	ZnO	3.38	54	7.81×10^{-3}	0.997
2	Zn _{0.99} Cu _{0.01} O	3.31	56	7.93×10^{-3}	0.995
3	Zn _{0.97} Cu _{0.03} O	3.30	60	8.71×10^{-3}	0.998
4	Zn _{0.95} Cu _{0.05} O	3.27	61	9.34×10^{-3}	0.997

come in contact with atmospheric oxygen and water, they react to give ROS like superoxide anion radical and hydroxide radical (Teichner and Formenti 1985).



And can further lead to generation of hydroperoxyl and hydrogen peroxide (H₂O₂) radicals



These ROS are highly reactive; hence, the destruction of microorganism in air and water may be achieved when they are in contact with the surface of a metal oxide photocatalyst. The resultant reaction between ROS and organic compounds leads to mineralization with formation of CO₂ and H₂O (Hoffmann et al. 1995).

Conclusion

Vernonia amygdalina leaf extract was successfully used to synthesize 0, 1, 3, and 5% Cu-doped ZnO NPs. The structural, morphological, and optical properties of the samples were investigated in details using XRD, SEM, EDX, UV-visible, and FT-IR spectroscopy. It can be seen that all the samples were crystalline in nature with wurtzite hexagonal structure and their crystallite size increases from 34 to 39 nm as Cu content increased from 0 to 5%. The lattice parameter “a” and “c” were found to be between 3.250 and 3260 Å and 5.307 and 5.323 Å, respectively. The atomic packing fraction of the samples was found to be 74.04%, and the bond length was between 1.990 and 1.996 Å. The Energy band gap was found to decline from 3.35 to 3.27 eV as Cu concentration was raised from 0 to 5%. The FT-IR study clearly

revealed the presence of reducing, stabilizing, and capping molecules present in VA. The antibacterial investigation showed that selected pathogens were all sensitive to the prepared samples; however, Cu-doped ZnO NPs showed better antibacterial activities across the selected pathogens. Photocatalytic activities of Zn_{0.97}Cu_{0.03}O and Zn_{0.95}Cu_{0.05}O had better percentage degradation efficiency (60 and 61%) and kinetic rate constant (8.71×10^{-3} and 9.34×10^{-3}) after 100 min of irradiation.

Acknowledgements The authors are thankful to Nano Research Group, UNN, and National Orthopedic Hospital Enugu, for giving us access to their Laboratory and to iThemba LABS, South Africa for XRD analysis.

Authors’ contributions Okeke IS, Agwu KK, and Ubachukwu AA: conceptualization. Okeke IS and Ezema FI: original draft, review and editing, methodology, investigation, data curation, and formal analysis. Agwu KK, Ubachukwu AA, and Ezema FI: supervision. Ezema FI and Maazu M: characterization and interpretation of data (XRD, EDS, and SEM). Ezema FI: validation. Okeke IS: writing the manuscript. Agwu KK, Ubachukwu AA, and Ezema FI: reviewing and editing the manuscript.

Funding information This research did not receive any specific grant from funding agencies in the public, commercial, or not-for-profit sectors. Data Availability All relevant data are available.

Compliance with ethical standards

Conflict of interest The authors declare that they have no conflict of interest.

References

Ahmad M, Pan C, Yan W, Zhu J (2010) Effect of Pb-doping on the morphology, structural and optical properties of ZnO nanowires synthesized via modified thermal evaporation. Mater Sci Eng 174:55–58

Alara OR, Abdurahman NH, Ukaegbu IC (2019) Extraction and characterization of bioactive compounds in *Vernonia amygdalina* leaf ethanolic extract comparing Soxhlet and

- microwave assisted extraction techniques. *J Taibah Univ Sci* 13: 414–422. <https://doi.org/10.1080/16583655.2019.1582460>
- Amrita KS, Randhawa GS, Singh R (2017) Synthesis and structural analysis of cobalt doped zinc nanoparticles. *IOSR J Appl Phys* 9:18–24
- Anastas PT, Warner JC (1998) Green chemistry: theory and practice. Oxford University Press, New York
- Aysaa NH, Salmanb HD (2016) Antibacterial activity of modified zinc oxide nanoparticles against *Pseudomonas aeruginosa* isolates of burn infections. *World Sci News* 33:1–14
- Bacterial cell structure (n.d.) In Wikipedia. Retrieved August 13, 2020, from <https://blog.apastyle.org/apastyle/2009/10/how-to-cite-wikipedia-in-apa-style.html>
- Bak T, Nowotny J, Rekas M, Sorrell CC (2002) Photoelectrochemical hydrogen generation from water using solar energy. Materials-related aspects. *Int J Hydrog Energy* 27: 1022–27991
- Bala N, Saha S, Chakraborty M, Maiti M, Das S, Basu R, Nandy P (2014) Green synthesis of zinc oxide nanoparticles using *Hibiscus subdariffa* leaf extract: effect of temperature on synthesis, anti-bacterial activity and antidiabetic activity. *RSC Adv* 5:4993–5003. <https://doi.org/10.1039/C4RA12784F>
- Bhuyan T, Mishra K, Khanuja M, Prasad R, Varma A (2005) Biosynthesis of zinc oxide nanoparticles from *Azadirachta indica* for antibacterial and photocatalytic applications. *Mater Sci Semicond Process* 32:55–61
- Ca FF, Xin S, Guo YG, Wan J (2011) Wet chemical synthesis of Cu/TiO₂ Nanocomposites with integrated Nano-current collectors as high rate anode materials in lithium-ion batteries. *Phys Chem Chem Phys* 13:2014–2020. <https://doi.org/10.1039/c0cp01119c>
- Chauhana R, Kumar A, Chaudharya RP (2010) Synthesis and characterization of copper doped ZnO nanoparticles. *J Chem Pharm Res* 2:178–183
- Chithra MJ, Pushpanathan K (2016) Thermal, structural and optical investigation of Cu-doped ZnO nanoparticles. *Mod Phys Lett B* 30:504–506
- Cong CJ, Hong JH, Liu QY, Liao L, Zhang KL (2006) Synthesis, structure and ferromagnetic properties of Ni doped ZnO nanoparticles. *Solid State Commun* 138:511–515
- Dao DV, van den Brecht M, Koeller Z, Le TK (2016) Effect of metal ion doping on the optical properties and the deactivation of photocatalytic activity of ZnO nanopowder for application in sunscreens. *Powder Technol* 288:366–370. <https://doi.org/10.1016/j.powtec.2015.11.030>
- Donlan RM (2008) Biofilms on central venous catheters: is eradication possible? *Curr Top Microbiol Immunol* 322:133–161. https://doi.org/10.1007/978-3-540-75418-3_7
- Dutta RK, Nenavathu BP, Gangishetty MK, Reddy AVR (2012) Studies on antibacterial activity of ZnO nanoparticles by ROS induced lipid peroxidation. *Colloids Surf B: Biointerfaces* 94:143–150. <https://doi.org/10.1016/j.colsurfb.2012.01.046>
- Edeoga HO, Okwu DE, Mbaebie B (2005) Phytochemical constituents of some Nigerian medicinal plants. *Afr J Biotechnol* 4:685–688
- Fabbiyola S, Kennedy LJ, Aruldoss U, Bououdina M, Dakhel AA, Vijaya JJ (2015) Synthesis of Co-doped ZnO nanoparticles via co-precipitation: structural, optical and magnetic properties. *Powder Technol* 286:757–765. <https://doi.org/10.1016/j.powtec.2015.08.054>
- Ganesan S, Babu IG, Mahendran D, Arulselvi PI, Elangovan N, Geetha N, Venkatachalam P (2016) Green engineering of titanium dioxide nanoparticles using *Ageratina altissima* (L.) King & H.E. Robines. medicinal plant aqueous leaf extracts for enhanced photocatalytic activity. *Ann Phytomedicine An Int J* 5:69–75. <https://doi.org/10.21276/ap.2016.5.2.8>
- George S, Pokhrel S, Xia T, Gilbert B, Ji Z, Schowalter M, Rosenauer A, Damoiseaux R, Bradley KA, Madler L (2009) Use of a rapid cytotoxicity screening approach to engineer a safer zinc oxide nanoparticle through iron doping. *ASC Nano* 4:15–29. <https://doi.org/10.1021/nn901503q>
- Gubin SP (2009) Biomedical applications of magnetic nanoparticles, Wiley-VCH Verlag GmbH & Co. KGaA. <https://doi.org/10.1002/9783527627561>
- Hajipour MJ, Fromm KM, Ashkarran AA, Jimenez de Aberasturi DRT, Larramendi IR, Jojo T, Serpooshan V, Mahmoudi J (2012) Antibacterial properties of nanoparticles. *Trends Biotechnol* 30:499–511
- Hamberg I, Granqvist CG (1986) Evaporated Sn-doped In₂O₃ films: basic optical properties and applications to energy-efficient windows. *J Appl Phys* 60:123–160
- Handago DT, Zereffa EA, Gonfa BA (2019) Effects of *Azadirachta indica* leaf extract, capping agents, on the synthesis of pure and Cu doped ZnO-nanoparticles: a green approach and microbial activity. *Open Chem* 17:246–253. <https://doi.org/10.1515/chem-2019-0018>
- Health Protection Agency (2012) English national point prevalence survey on healthcare-associated infections and antimicrobial use, Preliminary data
- Hoffmann MR, Martin ST, Choi W, Bahnemann DW (1995) Environmental applications of semiconductor photocatalysis. *Chem Rev* 95:69–96. <https://doi.org/10.1021/cr00033a004>
- Hong RY, Li JH, Chen LL, Liu DQ, Li HZ, Zheng Y, Ding J (2009) Synthesis, surface modification and photocatalytic property of ZnO nanoparticles. *Powder Technol* 189:426–432. <https://doi.org/10.1016/j.powtec.2008.07.004>
- Ijaz F, Shahid S, Khan SA, Ahmad W, Zaman S (2017) Green synthesis of copper oxide nanoparticles using *Abutilon indicum* leaf extract: antimicrobial, antioxidant and photocatalytic dye degradation activities. *Trop J Pharm Res* 16:743
- Imaga NOA, Bamigbetan DO (2013) In vivo biochemical assessment of aqueous extracts of *vernonia amygdalina* (bitter leaf). *Int J Nutr Metab* 5:22–27
- International Standard Organisation (2010) “Fine ceramics (advanced ceramics, advanced technical ceramics) determination of photocatalytic activity of surfaces in an aqueous medium by degradation of methylene blue,” Tech. Rep., ISO 10678, ISO Geneva: Switzerland
- Ju-Nam Y, Lead J (2008) Manufactured nanoparticles: an overview of their chemistry, interactions and potential environmental implications. *Sci Total Environ* 400:396–414
- Kathiresan K, Manivannan S, Nabeel A, Dhivya B (2009) Studies on silver nanoparticles synthesized by a marine fungus,

- Penicillium fellutanum* isolated from coastal mangrove sediment. *Colloids Surf B: Biointerfaces* 71:133–137
- Kaur P, Kumar S, Negi NS, Rao SM (2015) Enhanced magnetism in Cr-doped ZnO nanoparticles with nitrogen co-doping synthesized using sol–gel technique. *Appl Nanosci* 5:367–372
- Kesah CN, Egri-Okwaji MT, Iroha E (2004) Aerobic bacterial nosocomial infections in paediatric surgical patients at a tertiary health institution in Lagos, Nigeria, Niger. *Postgrad Med J* 11:4–9
- Khan SA, Noreen F, Kanwal S, Hussain G (2017) Comparative synthesis, characterization of Cu-doped ZnO nanoparticles and their antioxidant, antibacterial, antifungal and photocatalytic dye degradation activities. *Dig J Nanomater Biostructures* 12:877–889
- Labhane P, Huse V, Patle L, Chaudhari A (2015) Synthesis of Cu doped ZnO nanoparticles crystallographic, optical FTIR, morphological and photocatalytic study. *J Mater Sci Chem Eng* 3:39–51
- Lakshmeesha TR, Sateesh MK, Daruka B, Prasad SC, Sharma D, Kavyashree D, Chandrasekhar M, Nagabhushana H (2014) Reactivity of crystalline ZnO superstructures against fungi and bacteria pathogens: synthesized using *Nerium oleander* leaf extract. *Cryst Growth Des* 14:4068–4079
- Li L, Wang W, Liu H, Liu X, Song Q, Ren S (2009) First principles calculations of electronic band structure and optical properties of Cr-doped ZnO. *J Phys Chem C* 113:8460–8464. <https://doi.org/10.1021/jp811507r>
- Ma Z, Ren F, Ming X, Long Y, Volinsky AA (2019) Cu-doped ZnO electronic structure and optical properties studied by first-principles calculations and experiments. *Materials*. 12: 196. <https://doi.org/10.3390/ma12010196>
- Mohan R, Krishnamoorthy K, Kim S (2012) Enhanced photocatalytic activity of Cu-doped ZnO nanorods. *Solid State Commun* 154:375–380. <https://doi.org/10.1016/j.ssc.2011.12.008>
- NCCLS (2002) Methods for dilution antimicrobial susceptibility tests of bacteria that grow aerobically. Approved Standard M100-S12. Wayne, PA
- Nirmala GA, Pandian K (2007) Antibacterial efficacy of aminoglycosidic antibiotics protected gold nano-particles a brief study. *Colloids Surfaces A Physicochem Eng Asp* 297: 63–70
- Parthiban C, Sundaramurthy N (2015) Biosynthesis, characterization of ZnO nanoparticles by using *Pyrus pyrifolia* leaf extract and Their photocatalytic activity. *Int J Innovative Res Sci, Eng Tech* 4:9710–9718. <https://doi.org/10.15680/IJIRSET.2015.0410031>
- Peng Z, Wu D, Wang W, Tan F, Wang X, Chen J, Qiao X (2017) Effect of metal ion doping on ZnO nanopowders for bacterial inactivation under visible-light irradiation. *Powder Technol* 315:73–80. <https://doi.org/10.1016/j.powtec.2017.03.052>
- Rafaie HA, Nor R, Amin YM (2015) Magnesium doped ZnO nanostructures synthesis using *citrus aurantifolia* extracts: structural and field electron emission properties. *Mater Express* 5:226–232. <https://doi.org/10.1166/mex.2015.1227>
- Rouchdi M, Salmani E, Fares B, Hassanain N, Mzerd A (2017) Synthesis and characteristics of Mg doped ZnO thin films: experimental and ab-initio study. *Results Phys* 7:620–627
- Sajjad M, Ullaha I, Khanb MI, Khanc J, Khana MY, Qureshid MT (2018) Structural and optical properties of pure and copper doped zinc oxide nanoparticles. *Results Phys* 9:1301–1309
- Samadi M, Zirak M, Naseri A, Khorashadizade EM (2016) Recent progress on doped ZnO nanostructures for visible-light photocatalysis. *Thin Solid Films* 605:2–19
- Senthilkumar SR, Sivakumar T (2014) Green tea (*Camellia sinensis*) mediated synthesis of zinc oxide (ZnO) nanoparticles and studies on their antimicrobial activities. *Int J Pharm Pharm Sci* 6:461–465
- Shahid S, Khan SA, Ahmad U, Fatima S, Knawal S (2018) Size-dependent bacterial growth inhibition and antibacterial activity of Ag-doped ZnO nanoparticles under different atmospheric conditions. *Indian J Pharm Sci* 80:173–180
- Siddiqi KS, Husen A (2017) Recent advances in plant-mediated engineered gold nanoparticles and their application in biological system. *J Trace Elem Med Biol* 40:10–23
- Singh S, Srivastava VC, Lo SL, Mandal TK, Naresh G (2017) Morphology-controlled green approach for synthesizing the hierarchical self-assembled 3D porous ZnO superstructure with excellent catalytic activity. *Microporous Mesoporous Mater* 239:296–309
- Sirelkhatim A, MahmudS SA, Kaus NHM, Ann LC, Bakhori SKM, Hasan H, Mohamad D (2015) Review on zinc oxide nanoparticles: antibacterial activity and toxicity mechanism. *Nano-Micro Lett* 7:219–242. <https://doi.org/10.1007/s40820-015-0040-x>
- Song W, Zhang J, Guo J, Zhang J, Ding F, Li L, Sun Z (2010) Role of the dissolved zinc ion and reactive oxygen species in cytotoxicity of ZnO nanoparticles. *Toxicol Lett* 199:389–397. <https://doi.org/10.1016/j.toxlet.2010.10.003>
- Teichner SJ, Formenti M (1985) Photoelectrochemistry, Photocatalysis and Photoreactor, edited by Schiavello, M. Reidel, Dordrecht
- Thaweesaenga N, Supankit S, Techidheeraa W, Pecharapa W (2013) Structure properties of as-synthesized Cu-doped ZnO nanopowder synthesized by co-precipitation method. *Energy Procedia* 34:682–688
- Ullah R, Dutta J (2008) Photocatalytic degradation of organic dyes with manganese-doped ZnO nanoparticles. *J Hazard Mater* 156:194–200. <https://doi.org/10.1016/j.jhazmat.2007.12.033>
- Vegard L (1921) Die Konstitution der Mischkristalle und die Raumfüllung der Atome. *Z Phys* 307(5):17
- Vidya C, Hirematha S, Chandraprabhab MN, Antonyraja LMA, Gopala IV, Jaina A, Bansala K (2013) Green synthesis of ZnO nanoparticles by *Calotropis Gigantea*. *Int J Curr Engg Technol* 118–120
- Wang R, Xin JH, Yang Y, Liu H, Xu L, Hu J (2004) The characteristics and photocatalytic activities of silver doped ZnO nanocrystallites. *Appl Surf Sci* 227:312–317
- Wang J, Yang J, Li X, Feng B, Wei B, Wang D, Zhai H, Song H (2015) Effect of surfactant on the morphology of ZnO nanopowders and their application for photodegradation of rhodamine B. *Powder Technol* 286:269–275. <https://doi.org/10.1016/j.powtec.2015.08.030>
- World.Health.Organization (2016) The burden of health care-associated infection worldwide. Retrieved June 11th, 2018 from http://www.who.int/gpsc/country_work/burden_hcai/en/

- Yadav HK, Sreenivas K, Katiyar RS, Gupta V (2007) Defect induced activation of Raman silent modes in RF co-sputtered Mn doped ZnO thin films. *J PhysD Appl Phys* 40:6005–6009
- Yedurkar S, Maurya C, Mahanwar P (2016) Biosynthesis of zinc oxide nanoparticles using *Ixora Coccinea* leaf extract—a green approach. *Open J Synth Theory Appl* 5:1–14. <https://doi.org/10.4236/ojsta.2016.51001>
- Yousef JM, Danial EN (2012) *In vitro* anti-bacterial activity and minimum inhibitory concentration of ZnO NPs against pathogenic strains. *J Health Sci* 2:38–42
- Zhong JB, Li JZ, He XY, Zeng J, Lu Y, Hu W, Lin K (2012) Improved photocatalytic performance of Pd-doped ZnO. *Curr Appl Phys* 12:998–1001

Publisher's note Springer Nature remains neutral with regard to jurisdictional claims in published maps and institutional affiliations.